

# The triple Leidenfrost effect: preventing coalescence of drops on a hot plate

F. Pacheco-Vázquez,<sup>1</sup> R. Ledesma-Alonso,<sup>2</sup> J. L. Palacio-Rangel,<sup>1</sup> and F. Moreau<sup>3</sup>

<sup>1</sup>*Instituto de Física, Benemérita Universidad Autónoma de Puebla, A. P. J-48, Puebla 72570, Mexico*

<sup>2</sup>*Universidad de las Américas Puebla, San Andrés Cholula, C.P. 72810, Puebla, Mexico.*

<sup>3</sup>*Institut Pprime, UPR 3346 CNRS, ENSMA, Université de Poitiers, Futuroscope Cedex, France*

(Dated: November 11, 2021)

We report on the collision-coalescence dynamics of drops in Leidenfrost state using liquids with different physicochemical properties. Drops of the same liquid deposited on a hot concave surface coalesce practically at contact, but when drops of different liquids collide, they can bounce several times before finally coalescing when the one that evaporates faster reaches a size similar to its capillary length. The bouncing dynamics is produced because the drops are not only in Leidenfrost state with the substrate, they also experience Leidenfrost effect between them at the moment of collision. This happens due to their different boiling temperatures, and therefore, the hotter drop works as a hot surface for the drop with lower boiling point, producing three contact zones of Leidenfrost state simultaneously. We called this scenario *the triple Leidenfrost effect*.

A liquid droplet deposited on a solid substrate considerably hotter than the liquid boiling temperature,  $T_B$ , levitates on its own vapor, reducing its evaporation rate and the friction with the substrate. This widely studied phenomenon is called Leidenfrost effect [1, 2]. The minimum temperature  $T_L$  required to observe such scenario depends on the liquid and substrate properties [3–6]. For instance, a water drop enters in Leidenfrost state on a polished aluminum plate at  $T_L \approx 160 - 200^\circ\text{C}$  [6, 7]. In contrast, an ethanol droplet exhibits the Leidenfrost transition on a heated oil pool when the difference in temperatures,  $T_L - T_B$ , is only of a few degrees [8], revealing that a slight superheating can be enough to observe droplet levitation on a liquid surface. Recently, different dynamics involving the Leidenfrost effect have been explored: self-propelled droplets [9, 11], sustained rotation [12, 13], star-shaped oscillations [7, 14, 15], inverted Leidenfrost [16], bouncing hydrogel balls [17], exploding droplets [18], etc. These studies suggest possible applications of the Leidenfrost mechanism in engineering and microfluidics. However, we need to understand first how Leidenfrost drops of distinct liquids interact.

When two droplets of the same liquid collide, they coalesce if the gas film between them is drained during the collision time. At room temperature, different regimes of bouncing, coalescence and separation in two-droplets collisions are well known depending on the Weber number (the ratio of collision energy to surface energy), impact parameter (the deviation of the droplets trajectories from that of head-on impact), and droplets size ratio [19–23]. The dynamics also depends on liquids miscibility [24–26]: a water droplet coalesces with an ethanol droplet [25] but it can bounce against an oil droplet [26]. On non-wetting surfaces, two micrometric droplets may coalesce, bounce or propel, due to the transfer of surface energy to mechanical energy [27, 28]. The temperature effect on the outcome of two water droplets collisions was only recently considered [29–31]: an increase in temperature for both or one of the droplets increases the possibility of coalescence [29], and self-propelled jumping upon coalescence occurs for water droplets in Leidenfrost state [27, 30], as

in the case of drops on superhydrophobic surfaces [27]. Although droplets of distinct liquids interact and collide with overheated surfaces in several processes (e.g. fuel-oxidizer spray systems and composite fuels combustion [25, 32–34]), the collision outcome for two Leidenfrost droplets of unlike liquids remained so far unexplored.

In this letter, we study for the first time the collision and coalescence of two Leidenfrost drops of different miscible and immiscible liquids. First, we determined the Leidenfrost temperature  $T_L$  for each liquid. Then, we focused on the collision of two large drops on a hot concave plate at temperature  $T_p > T_L$ . When two drops collide, they coalesce directly or bounce repeatedly depending on the difference of the liquids boiling temperatures  $\Delta T$ , see Movie [35]. The bouncing dynamics can be explained assuming that the Leidenfrost effect also occurs between droplets with large  $\Delta T$ , generating a vapor layer that prevents coalescence. After one droplet evaporates and reaches a size similar to its capillary length, the drops coalesce regardless of their initial volumes, impact velocity and plate temperature. Striking scenarios follow the coalescence: miscible droplets rapidly mix, immiscible droplets form a multiphasic Leidenfrost drop with one liquid covering the other, and a volatile droplet explodes violently inside the hotter larger drop.

*Experimental procedure.*— We placed on a hotplate a polished cylindrical aluminum substrate (15 cm diameter, 4 cm thickness, roughness  $< 0.5 \mu\text{m}$ ) machined radially with a small angle ( $\phi = 2^\circ$ ), in order to keep the droplets at the center of the substrate (to the eye, the surface looks flat). The plate temperature  $T_p$  was controlled with a solid state relay (SSR) and monitored with a K-type ATT29 thermocouple (TC). One or two drops of initial volume  $V_0 \in [100, 1000] \mu\text{l}$  of 11 low viscosity liquids with different physicochemical properties [35] were deposited on the plate using micropipettes, and the dynamics was filmed from the top with a high speed camera Photron SA3 (see Fig. 1 and more details in SI [35]).

*One droplet evaporation.*— To determine the Leidenfrost temperature for each liquid, we measured the evaporation time  $\tau$  of  $500 \mu\text{l}$  droplets at different plate temper-

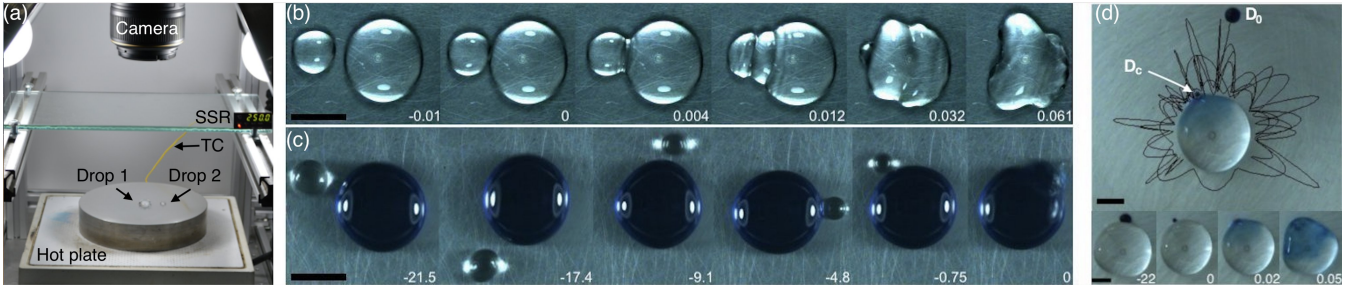


FIG. 1. a) Experimental setup. b) Direct coalescence of two water droplets in Leidenfrost state. c) Consecutive bouncing of an ethanol droplet (transparent one) against a water droplet (tinted with methylene blue) during several seconds before coalescing. d) Path of an acetonitrile droplet (tinted in blue) bouncing several times against a water drop. The snapshots show that the water droplet, initially transparent, turns bluish suddenly when the droplets coalesce. In (b-d), the elapsed time is indicated in seconds in each snapshot, with  $t=0$  s corresponding to the moment of coalescence [scale bars: (b-c) 10 mm, (d) 5 mm].

atures  $T_p$ . An abrupt increase of  $\tau(T_p)$  occurs at  $T_p \approx T_L$  [2]. In Fig. 2a,  $\tau$  vs  $T_p$  is reported for water (red squares), in which case  $T_L \approx 210^\circ\text{C}$ . Similar plots were obtained for all liquids. For clarity, only the values of  $\tau(T_L)$  are shown (blue points). In most cases  $\tau(T_L) \sim 100 - 200$  s, but for water  $\tau(T_L) \sim 450$  s because its latent heat  $L$  is more than twice larger than the  $L$  values of the other liquids, see Table I. The value of  $T_L$  found for each liquid was plotted as a function of  $T_B$  in Fig. 2b. The data can be linearly scaled (see Fig. 2c) using the dimensionless temperatures proposed very recently in Ref. [36], given by  $\Theta_L = T_L C_p/L$  and  $\Theta_B = T_B C_p/L$ , where  $C_p$  is the gas specific heat. The linear fit (blue line) may provide a good estimate of  $T_L$  for an additional liquid deposited on the aluminum plate, if  $L$ ,  $C_p$  and  $T_B$  are known.

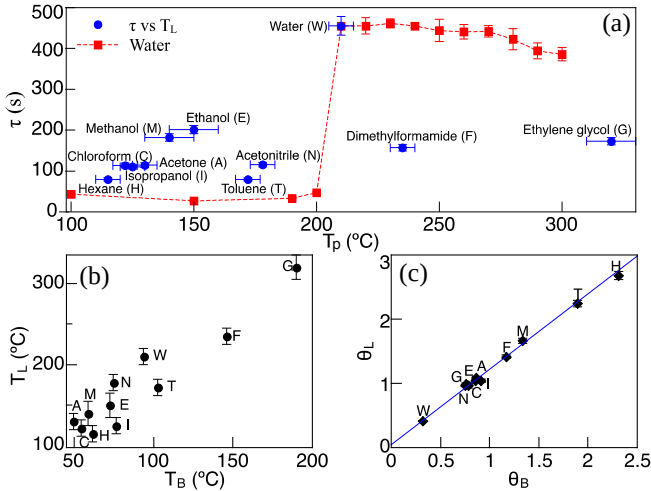


FIG. 2. a) Evaporation time  $\tau$  vs substrate temperature  $T_p$  [red squares] and  $\tau(T_L)$  [blue dots], for 0.5 ml drops of different liquids. b)  $T_L$  vs  $T_B$  and c)  $\Theta_L$  vs  $\Theta_B$ , for the liquids in (a), with the best linear fit:  $\Theta_L = 1.17\Theta_B + 0.05$  (see text).

*Collision of two drops.*- Once known  $T_L$  for each liquid, two drops of different liquids (labeled Drop1 and Drop2 in Fig. 1a) with boiling temperatures  $T_{B1}$  and  $T_{B2}$  were deposited on the aluminum plate at  $T_p = 250^\circ\text{C}$

( $T_p > T_L$  for both drops [37]). First, we placed Drop1 of volume  $V_0 = 1000 \mu\text{l}$  at the center of the plate. Then, Drop2 of  $V_0 \in [100, 700] \mu\text{l}$  was released close to the edge of the plate at  $d \sim 7$  cm from Drop1. Drop2 slides under the action of gravity  $g$  until colliding with Drop1 with impact velocity  $v \sim \sqrt{2gd \sin \phi} \approx 22$  cm/s. The collision is followed by two dynamics depending on the liquids pairs: i) direct coalescence, or ii) consecutive rebounds before coalescence. The direct coalescence lasts some milliseconds [Fig. 1b], and it was observed mainly with drops of the same liquid (e.g. water-water) or liquids with similar properties (e.g. ethanol-isopropanol). In contrast, drops with large differences in properties (e.g. water-ethanol or water-acetonitrile) remain bouncing during several seconds, or even minutes, while they evaporate until reaching a critical size to finally coalesce [Figs. 1c-d]. Table I summarizes our findings based on the dominant dynamics observed in at least five repetitions. Note that drops of the same liquid coalesce directly, almost all liquids bounce against water or dimethylformamide, alcohols coalesce between them, and three pairs (acetonitrile with acetone or toluene, and toluene with isopropanol) can either coalesce or bounce. For immiscible liquids, the drops can bounce (e.g. hexane with water) or merge directly (toluene with water), but at the end the liquids remain unmixed forming a single Leidenfrost drop.

Since working with all the above combinations is complex due to the wide variety of liquid properties, we focus the following discussion in experiments with a Drop1 of 1 ml of water, interacting with a Drop2 of 250  $\mu\text{l}$  of another liquid (their properties are labelled with a subindex 1 and 2, respectively). For these combinations, we measured the time  $t_c$  from Drop2 deposition until its coalescence with Drop1. Then, we realized that two parameters could possibly be used to determine the conditions for direct coalescence ( $t_c \sim 0$ ) or bouncing ( $t_c \gg 0$ ): the difference of surface tensions  $\Delta\sigma = \sigma_1 - \sigma_2$ , see Fig. 3a, or the difference in boiling temperatures  $\Delta T_B = T_{B1} - T_{B2}$ , see Fig. 3b. Note in these plots the transition from direct coalescence to bouncing at  $\Delta\sigma \approx 31$  mN/m, and at  $\Delta T_B \approx 15^\circ\text{C}$ , respectively (dashed lines). Additionally,

Liquid	$T_B$ °C	$L$ kJ/kg	$\sigma$ mN/m	$\lambda_c$ mm	Drop 1	Drop 2											
						W	E	M	I	A	H	C	N	T	F		
Water	93	2256	59	2.5	W	c	r	r	r	r	$r_{(i)}$	$r_{(i)}$	r	$c_{(i)}$	c		
Ethanol	72	846	17	1.5	E	r	c	c	c	c	r	c	c	r	r		
Methanol	59	1100	19	1.6	M	r	c	c	c	c	$r_{(i)}$	r	c	r	r		
Isopropanol	76	779	16	1.5	I	r	c	c	c	c	r	c	c	c/r	r		
Acetone	50	518	19	1.7	A	r	c	c	c	c	r	c	c/r	r	r		
Hexane	61	338	13	1.5	H	$r_{(i)}$	r	$r_{(i)}$	r	r	c	c	$r_{(i)}$	r	$r_{(i)}$		
Chloroform	54	247	22	1.3	C	$r_{(i)}$	c	r	c	c	c	c	c	c	r		
Acetonitrile	74	729	22	1.8	N	r	c	c	c	c/r	$r_{(i)}$	c	c	c/r	r		
Toluene	103	365	18	1.5	T	$c_{(i)}$	r	r	c/r	r	r	c	c/r	c	r		
DFormamide	146	546	22	1.6	F	c	r	r	r	r	$r_{(i)}$	r	r	r	c		

TABLE I. Outcome of the collision of two Leidenfrost drops for different liquids pairs [38]: direct coalescence (**c**), consecutive rebound (**r**) or both scenarios (**c/r**). A subindex (*i*) indicates immiscible liquids [39]. The latent heat  $L$ , surface tension  $\sigma$  and capillary length  $\lambda_c$  of each liquid at the boiling temperature  $T_B$  are reported (values in Puebla, Mexico, at  $\sim 2200$  m above the sea level). Data based on Refs. [39–42].

we performed experiments using mixtures of water and ethanol for Drop2 (open symbols), reducing progressively  $\sigma_2 \approx 59$  mN/m and  $T_{B2} \approx 93^\circ\text{C}$  for pure water, in which case Drop2 coalesces directly with Drop1 (same liquid), until attaining an ethanol concentration of 33%, at which Drop2 exhibits bouncing before coalescence. For this concentration,  $\sigma_2 \approx 28$  mN/m and  $T_{B2} \approx 78^\circ\text{C}$  [40], which corresponds to  $\Delta\sigma \approx 31$  mN/m and  $\Delta T_B \approx 15^\circ\text{C}$ . These transition values are in agreement with those found using different liquids. One can notice in Fig. 3 that toluene and dimethylformamide (with  $t_c = 0$  s) are beyond the transition for  $\Delta\sigma$  but appear in the right side considering  $\Delta T_B$ . This suggests that  $\Delta T_B$  determines if two droplets bounce or coalesce. Let us analyze the bouncing dynamics to get more insights about the dominant mechanism.

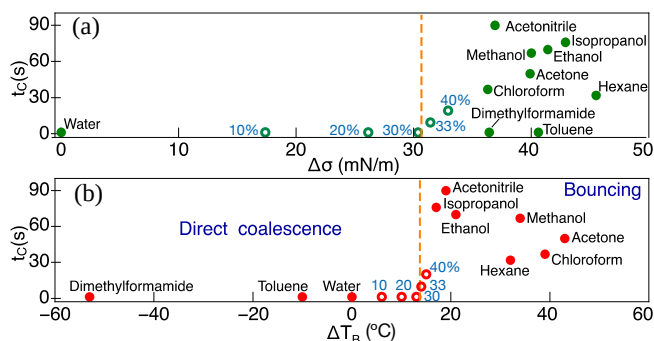


FIG. 3. Coalescence time  $t_c$  for a  $250 \mu\text{l}$  Drop2 of the indicated liquids with a  $1 \text{ ml}$  Drop1 of water as a function of: a)  $\Delta\sigma$ , and b)  $\Delta T$ . Blue numbers denote the ethanol concentration (%) in Drop2 composed of water-ethanol mixtures.

*Bouncing dynamics and coalescence size:* We performed particle tracking from videos taken at 60 fps focused on Drop2 (of different liquids) bouncing against Drop1 (water). An example of this dynamics is shown

in Fig. 1d for acetonitrile during the last 22 s before coalescing with water. The moment of coalescence corresponds to  $t = 0$  s. Figure 4a shows the radial position of Drop2,  $r_b$ , measured from the surface of Drop1 for different liquids: isopropanol performs the largest rebounds and chloroform the smallest ones. Note that the bouncing lengths are erratic, indicating that the moment of coalescence is independent of the impact velocity in the studied range. The erratic bouncing also indicates that the rebound velocity can be even higher than the impacting velocity, which is possible if the vapor layer is constantly replenished by the evaporation of the Leidenfrost droplets during the collision time [30]. This could also explain the remarkable difference between our results and those reported in the literature for drops at ambient temperature [25]. If one takes for example the Drop2 of ethanol (density  $\rho = 0.748 \text{ g/cm}^3$ , initial diameter  $D_2 \sim 1.5 \text{ cm}$ ) that bounces different radial distances with  $v \approx 0 - 22 \text{ cm/s}$  and impact parameter  $X \sim 0$ , the Weber number,  $We = \rho v^2 D_2 / \sigma$ , is in the range  $0 < We < 46$ . At room temperature and similar Weber numbers, a water drop always coalesces with an ethanol drop [25], whereas in Leidenfrost state, we observed repeated bouncing.

Figure 4b shows that, for all liquids, the diameter  $D_2$  of Drop2 decreases linearly with time due to evaporation until coalescing at  $t = 0$  s, with coalescence size  $D_c \sim 1 - 2 \text{ mm}$ . This linear dependence, with slope  $k = -dD_2(t)/dt$  given by the liquid evaporation rate (gray lines), is in agreement with Ref [8] for the evaporation of a single Leidenfrost drop on a heated liquid pool, and it contrasts with the power-law model derived in Ref. [2] for individual water drops. Furthermore,  $D_c$  is largely independent of the initial volume of Drop2 in the range  $V_0 \in [100, 700] \mu\text{l}$ , as shown in Fig. 4c (solid symbols). The dashed red line indicates the diameter  $D_0$  (viewed from above) of a drop with pancake-like shape and initial volume  $V_0$ ; the drops evaporate and decrease linearly in size from  $D_0$  until reaching a size  $D_c$ , of the order of the liquids capillary lengths,  $\lambda_c = (\sigma/\rho g)^{1/2}$  (see values in Table I). The initial volume of the larger Drop1 is also not relevant for the coalescence size of Drop2. Figure 4d shows the case of methanol droplets of different initial volumes coalescing with water drops of 0.5, 1.0 and 1.5 ml. The coalescence time for a given  $V_0$  is the same in the three cases, indicating that  $t_c$  only depends on the volume of Drop2, i.e., when it reaches a given diameter  $D_2 = D_c$ , regardless of the diameter of the central drop  $D_1$  [the equivalent coalescence diameter is  $D_{eq} = D_1 D_2 / (D_1 + D_2)$ , since  $D_2 \ll D_1$ , then  $D_{eq} \sim D_2$ , i.e., the smaller drop essentially interacts with a flat surface]. As shown in Fig. 4d,  $t_c$  follows a power-law dependence on  $V_0$  similar to the one described previously for the lifetime of a single Leidenfrost drop [43]. Remarkably,  $D_c$  is also independent of the substrate temperature (for  $T_p > T_L$ ) as it is shown in Fig. 4e for experiments performed in the range of  $220^\circ\text{C} < T_p < 450^\circ\text{C}$ . Although only the case of methanol-water is shown in Figs. 4d-e, similar results were obtained using other liquids.

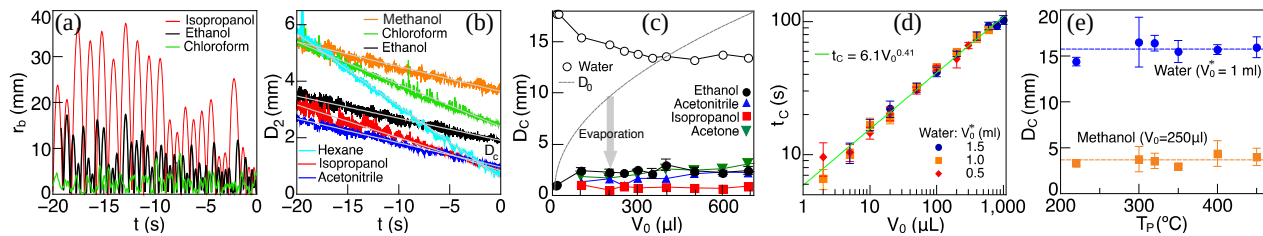


FIG. 4. a) Size of radial bounces  $r_b$  and b) diameter  $D_2$  of Drop2 as a function of time  $t$ , for drops of different liquids of initial volume  $V_0 = 250 \mu\text{L}$  before coalescing with water [for clarity, only the last 20 s of bouncing for some liquids are shown, with coalescence at  $t=0$  s. The evolution of  $D_2(t)$  during the complete process can be found in the Supplementary information [35]]. Gray lines exhibit the linear decrease of  $D_2$  vs  $t$ . c) Coalescence size  $D_c$  of a Drop2 as a function of  $V_0$  for different liquids. d) Log-log plot of  $t_c$  vs  $V_0$  of a Drop2 of methanol with a water Drop1 of three different initial volumes  $V_0^*$ . The green line highlights a power law behavior of the form  $t_c = aV_0^n$ . In (a)–(d), the experiments were performed at  $T_p = 250^\circ\text{C}$ . e) Size  $D_c$  of the methanol drop [Drop2] and the water drop [Drop1] when they coalesce, as a function of  $T_p$  ( $V_0$  and  $V_0^*$  are indicated).

*The triple Leidenfrost effect.*— Let us put the pieces together. For two drops to coalesce they must come into contact. Thus, the coalescence could be prevented if the thin gas layer between the droplets is replenished during the collision time by the vapor produced between each drop and the plate. However, this description fails in explaining why two Leidenfrost drops of the same liquid coalesce directly whereas drops of different liquids do not. We propose an alternative mechanism illustrated in Fig. 5a: when two droplets are deposited on a very hot plate at temperature  $T_p$ , both droplets levitate on their own vapor, experiencing independently the well known Leidenfrost effect. The temperature of each droplet is practically its boiling temperature [2]; in the sketch, Drop1 is at temperature  $T_{B1}$ , and Drop2 at temperature  $T_{B2}$ . For two drops of distinct liquids, one drop has a higher boiling point than the other one. Let say  $T_{B1} \gg T_{B2}$ . As in the case of droplet levitation on a liquid pool [8], Drop1 acts as a superheated surface for Drop2, and consequently, the Leidenfrost state is also established between the droplets, preventing coalescence. Therefore, there are three simultaneous zones of vapor-mediated levitation, indicated by L1, L2 and L3 in Fig. 5a. This also explains why two droplets of the same liquid coalesce directly, because in such a case  $T_{B1} = T_{B2}$  and the Leidenfrost effect between the droplets is not established. Moreover, if  $\Delta T_B$  is very small, the amount of vapor produced during the collision is not enough to avoid contact [44]. The vapor expelled from the bottom of the droplets cannot be the responsible of the frustrated coalescence for two reasons: 1) if that were the case, two droplets of the same liquid would also bounce, and 2)  $D_c$  would increase notably with  $T_p$  because more vapor is generated in the L1 and L2 zones at higher plate temperatures (but this is not the case as it was shown in Fig. 4e). A first attempt to determine the vapor produced in each zone and the coalescence size can be found in the supplementary information [35]. Here, we provide direct evidence of the existence of the L3 vapor layer. To produce visible amounts of vapor during the collision time, we performed an experiment using liquids with the largest  $\Delta T_B$  and using a Drop2 of the

most volatile liquid (lowest latent heat). Based on Table I [35], we used ethylene glycol ( $T_{B1} = 190^\circ\text{C}$ ) and chloroform ( $T_{B2} = 54^\circ\text{C}$ ,  $L = 247 \text{ kJ/kg}$ ). Figure 5b shows snapshots of the collision (see also Movie [35]). Clearly, a vapor layer is observed between the drops at the moment of collision, which prevents coalescence. We presume that the same mechanism is behind the frustrated coalescence for other pairs of liquids, but the vapor produced is scarce and cannot be easily visualized. Finally, when the smaller droplet decreases in size after several bounces and becomes spherical (i.e.  $D_2 \sim \lambda_c$ ), the vapor layer can be easily evacuated and the drops coalesce.

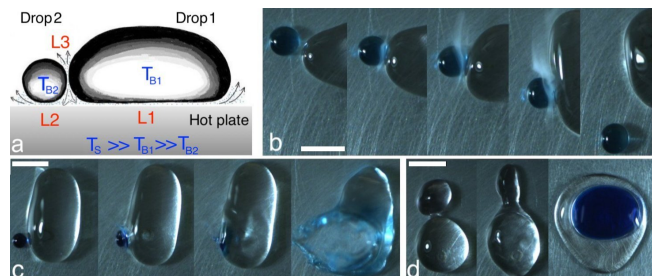


FIG. 5. a) Sketch of the triple Leidenfrost effect (see text). b) Snapshots taken at 500 fps showing the vapor layer generated when droplets of ethylene glycol (transparent) and chloroform (blue) collide ( $T_p = 350^\circ\text{C}$ ). c) Explosive coalescence of chloroform (blue) with ethylene glycol. d) Water (blue) and toluene join but remain unmixed (scale bars = 5 mm).

When two Leidenfrost drops finally coalesce, different scenarios occur. For ethylene glycol with a volatile liquid, like chloroform,  $\Delta T_B$  is so large that chloroform explodes violently after coalescence (Fig. 5c). Another striking scenario was observed for immiscible drops, indicated by (i) in Table I. For instance, water and toluene merge in a single Leidenfrost drop, but they remain unmixed with toluene covering the water drop (Fig. 5d). Methylene blue in water allows to confirm that there is no mass transfer between the droplets. This contrasts with miscible drops (Fig. 1d), where the transparent droplet becomes bluish only some milliseconds after coalescence.



In summary, this is the first systematic study focused on the collision of Leidenfrost drops of distinct liquids (miscible and immiscible). New scenarios of drops interactions and coalescence were revealed, which are remarkably different from those observed with drops at room temperature. Two Leidenfrost drops bounce one against the other when enough vapor is generated between them during the collision time; otherwise, the drops coalesce.

This study have possible applications for driving droplets in millimetric fluidic systems [22], for selective coalescence techniques (see Movie [35]), and also could help to improve our understanding of fuel drops interaction in overheated engines [32–34].

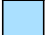
*Acknowledgements.*— Research supported by Conacyt Mexico through Frontier Science 2019 Program (Project: 140604), and Cátedra Marcos Moshinsky 2020. We acknowledge J. Pierron and L. Vallet for initial tests.

- 
- [1] J. G. Leidenfrost, *De aquae communis nonnullis qualitatibus tractatus* (Ovenius, 1756).
- [2] A.-L. Bianco, C. Clanet, and D. Quéré, *Physics of Fluids* **15**, 1632 (2003).
- [3] N. Nagai and S. Nishio, *Experimental Thermal and Fluid Science* **12**, 3 (1996).
- [4] H. Kim, B. Truong, J. Buongiorno, and L.-W. Hu, *Appl. Phys. Lett.* **98** 083121 (2011).
- [5] I. U. Vakarelski, N. A. Patankar, J. O. Marston, D.Y.C. Chan, S. T. Thoroddsen, *Nature* **489**, 274-277 (2012).
- [6] J. D. Bernardin, and I. Mudawar, *J. Heat Transfer* **124**, 864 (2002).
- [7] S. Hidalgo-Caballero, Y. Escobar-Ortega, F. Pacheco-Vázquez, *Phys. Rev. Fluids* **1**, 051902(R) (2016).
- [8] L. Maquet, B. Sobac, B. Darbois-Textier, A. Duchesne, M. Brandenbourger, A. Rednikov, P. Colinet, and S. Dorbolo, *Phys. Rev. Fluids* **1**, 053902 (2016).
- [9] G. Lagubeau, M. Le Merrer, C. Clanet, and D. Quéré, *Nature Phys.* **7**, 395 (2011).
- [10] C. Liu, K. Sun, C. Lu, J. Su, L. Han, Z. Wang, Y. Liu, *J. Colloid Interface Sci.* **569**, 229-234 (2020).
- [11] G. Graeber, K. Regulagadda, P. Hodel, C. Kuttel, D. Landolf, T. M. Schutzius, and D. Poulikakos, *Nat Commun* **12**, 1727 (2021).
- [12] P. Agrawal, G. G. Wells, R. Ledesma-Aguilar, G. McHale, A. Buchoux, A. Stokes, and K. Seane, *Applied Energy* **240**, 399 (2019).
- [13] A. Bouillant, T. Mouterde, P. Bourriane, A. Lagarde, C. Clanet, and D. Quéré, *Nature Phys.* **14**, 1188 (2018).
- [14] X. Ma, J.-J. Litor-Santos, and J. C. Burton, *Phys. Fluids* **27**, 091109 (2015).
- [15] P. Yi, P. Thurgood, N. Nguyen, H. Abdelwahab, P. Petersen, C. Gilliam, K. Ghorbani, E. Pirogova, S.-Y. Tang, and K. Khoshmanesh, *Soft Matter* **16**, 8854-8860 (2020).
- [16] J. O. Marston, I. U. Vakarelski, and S. T. Thoroddsen, *J. Fluid Mech.* **699**, 465-488 (2012).
- [17] S. R. Waitukaitis, A. Zuiderwijk, A. Souslov, C. Coullais, and M. Van Hecke, *Nature Physics* **13**, 1095 (2017).
- [18] F. Moreau, P. Colinet, and S. Dorbolo, *Phys. Rev. Fluids* **4**, 013602 (2019).
- [19] J. Qian and C. K. Law, *JFM* **331**, 59-80 (1997).
- [20] C. Tang, P. Zhang, and C. K. Law, *Physics of Fluids* **24**, 022101 (2012).
- [21] K.G. Krishnan, E. Loth, *Int. Journal of Multiphase Flow* **77**, 171-186 (2015).
- [22] J. Jin, C. Ooi, D. Dao, and N.-T. Nguyen, *Micromachines* **8**, 336 (2017).
- [23] K. H. Al-Dirawi, A. E. Bayly, *Exp Fluids* **61**, 50 (2020).
- [24] J.-T. Zhang, H.-R. Liu, and H. Ding, *Phys. Fluids* **32**, 082106 (2020);
- [25] T.-C. Gao, R.-H. Chen, J.-Y. Pu, and T.-H. Lin, *Exp. Fluids* **38**, 731 (2005).
- [26] R.-H. Chen and C.-T. Chen, *Exp. Fluids* **41**, 453 (2006).
- [27] J. B. Boreyko and C.-H. Chen, *Physics of Fluids* **22**, 091110 (2010).
- [28] O. Ramírez-Soto, V. Sanjay, D. Lohse, J. T. Pham, and D. Vollmer, *Science Advances* **6** (2020).
- [29] N. Yi, B. Huang, L. Dong, X. Quan, F. Hong, P. Tao, C. Song, W. Shang and T. Deng, *Sci. Rep.* **4**, 4303 (2014).
- [30] F. Liu, G. Ghigliotti, J. J. Feng, and C.-H. Chen, *J. Fluid Mech.* **752**, 22-38 (2014).
- [31] N.E. Shlegel, P.P. Tkachenko, and P.A. Strizhak, *Powder Technology* **367** 820-830 (2020).
- [32] A. E. Ashikhmin, N. A. Khomutov, M. V. Piskunov, and V. A. Yanovsky, *Appl. Sci.* **10**, 685 (2020).
- [33] S. Sen, V. Vaikuntanathan, and D. Sivakumar, *Int. J. Therm. Sci.* **121**, 99-110 (2017).
- [34] C. Cen, H. Wu, C. Lee, L. Fan, F. Liu, *Intl. J. Heat Mass Transfer* **132**, 130-137 (2019).
- [35] Supplementary Information and movies of collisions of two leidenfrost drops for different liquids combinations.
- [36] M.-A.J. van Limbeek, O. Ramírez-Soto, A. Prosperetti, and D. Lohse, *Soft Matter* **17**, 3207 (2021).
- [37] At this temperature, all the liquids listed in Table I exhibit Leidenfrost state on the aluminum plate.
- [38] Results obtained with drops of diameter  $D > \lambda_c$ .
- [39] Merck KGaA. Merck solvent miscibility chart (2020); <https://www.sigmaaldrich.com/chemistry/solvents/solvent-miscibility-table.html> [last accessed 01 December 2020]
- [40] G. Vázquez, E. Alvarez, and J. M. Navaza, *Journal of Chemical & Engineering Data* **40**, 611 (1995).
- [41] C. L. Yaws, *Chemical Properties Handbook* (McGraw-Hill Education), 1999.
- [42] <https://www.engineeringtoolbox.com>, Engineering Toolbox [online] (2001).
- [43] B. Sobac, A. Rednikov, S. Dorbolo, and P. Colinet, *Droplet Wetting and Evaporation* (Academic Press), pp. 85–99, 2015.
- [44] For dimethylformamide(DMF)-water ( $\Delta T_B \sim -53^\circ\text{C}$ ), it is the water drop the one that could reach the Leidenfrost state interacting with DMF, but the latent heat of water is so high that the vapor produced during the collision time is probably not enough to prevent coalescence.


# APPENDIX

## A. PROPERTIES OF FLUIDS

Drop 1	Drop 2									
	W	E	M	I	A	H	C	N	T	F
Water (W)						●	●		●	
Ethanol (E)										
Methanol (M)						●				
Isopropanol (I)										
Acetone (A)										
Hexane (H)	●		●					●		●
Chloroform (C)	●									
Acetonitrile (N)						●				
Toluene (T)	●									
Dformamide (F)						●				



Miscible



Immiscible

**Supplementary Table 1.** Miscibility chart for the liquids pairs used in this study. Data is based on Ref. [4].

Liquid	Boiling point	Surface tension	Density	Viscosity	Capillary length	Latent heat	Dipolar moment
	$T_B$ ( $^{\circ}\text{C}$ )	$\sigma$ (mN/m)	$\rho$ ( $\text{kg}/\text{m}^3$ )	$\eta$ (mPa/s)	$\lambda_c$ (mm)	$L$ (kJ/kg)	$D$ (D)
Water	93	59	940	0.284	2.5	2256	1.85
Ethanol	72	17	748	0.418	1.5	846	1.66
Methanol	59	19	725	0.296	1.6	1100	1.70
Isopropanol	76	16	724	0.523	1.5	779	1.55
Acetone	50	19	711	0.242	1.7	518	2.69
Hexane	61	13	615	0.201	1.5	338	0.09
Cholorform	54	22	1411	0.398	1.3	247	1.15
Acetonitrile	74	22	714	0.224	1.8	729	3.92
Toluene	103	18	780	0.419	1.5	365	0.36
D.Formamide	146	22	823	0.289	1.6	546	3.86
E.Glycol	190	23	1091	0.740	1.5	800	2.27

**Supplementary Table 2.** Some physicochemical properties of the liquids used in this study. The values are reported at the boiling temperature  $T_B$  in Puebla, Mexico, at 2200 masl. Data was estimated using Refs. [1–3].

Vapor	@ temperature $T_f = (T_B + T_p)/2$				@ temperature $T_{av} = (T_1 + T_2)/2$			
		Density	Viscosity	Thermal conductivity		Density	Viscosity	Thermal conductivity
	$T_f$ (°C)	$\rho$ (kg/m <sup>3</sup> )	$\eta$ ( $\mu$ Pa/s)	$k$ (mW/(m*K))	$T_{av}$ (°C)	$\rho$ (kg/m <sup>3</sup> )	$\eta$ ( $\mu$ Pa/s)	$k$ (mW/(m*K))
Water	171.5	0.378	15.073	31.267	93.0	0.459	11.808	24.416
Ethanol	161.0	0.990	12.658	29.405	82.5	1.208	10.520	20.709
Methanol	154.5	0.699	14.079	28.721	76.0	0.856	11.406	20.273
Isopropanol	163.0	1.285	11.464	30.219	84.5	1.567	9.341	22.604
Acetone	150.0	1.280	10.772	21.981	71.5	1.572	8.714	14.859
Hexane	155.5	1.875	9.367	26.735	77.0	2.295	7.659	17.673
Cholorform	152.0	2.619	14.488	9.499	73.5	3.212	11.873	7.677
Acetonitrile	162.0	0.880	10.363	18.705	83.5	1.074	8.538	13.662
Toluene	176.5	1.911	10.586	25.475	98.0	2.315	8.796	17.793
D. Formamide	198.0	1.447	10.322	20.949	119.5	1.736	8.416	15.334
E.Glycol	220.0	1.174	13.620	29.902	141.5	1.396	11.481	23.243

**Supplementary Table 3.** Some physicochemical properties of the vapors generated in this study. The values are reported at the film temperature  $T_f = (T_B + T_p)/2$  and at the average temperature  $T_{av} = (T_1 + T_2)/2$  in Puebla, Mexico, at 2200 masl. Data was estimated using Refs. [2].  $T_B$  is the boiling temperature for each fluid, reported in Supplementary Table 2.  $T_p = 250^\circ\text{C}$  is the plate temperature.  $T_{av}$  corresponds to the average temperature at the gap between the drops, which temperatures are  $T_1 = T_{B1}$  and  $T_2 = T_{B2}$  at the Leidenfrost state, considering that Drop1 is a water drop and Drop2 is made of the fluid in each row in the table.

## B. DROP SHAPE APPROXIMATION

A spherical shape is observed for drops with  $V \leq (4\pi/3)\lambda_c^3$ , whereas a puddle with pancake-like shape is observed for volumes  $V > (4\pi/3)\lambda_c^3$ . A drop in Leidenfrost state, that is placed over a horizontal plate, presents a projected diameter  $D$  view from above that depends on the volume  $V$  and the shape of the drop. For a spherical shape, the volume is directly related to the corresponding projected diameter, whereas for a pancake-like shape a height of approximately twice the capillary length  $2\lambda_c$ , the volume is calculated from the integral:

$$V = \int_{-\lambda_c}^{\lambda_c} r^2 dz \quad \text{with} \quad r(z) = \frac{D}{2} - \lambda_c + \sqrt{\lambda_c^2 - z^2}, \quad (1)$$

which leads to the following relationship:

$$V = 2\pi\lambda_c \left(\frac{D}{2} - \lambda_c\right)^2 + \pi^2\lambda_c^2 \left(\frac{D}{2} - \lambda_c\right) + \frac{4\pi}{3}\lambda_c^3. \quad (2)$$

Therefore, the reference diameter  $D_0$  should be estimated as follows:

$$D_0 \approx \begin{cases} 2\lambda_c \left(\frac{3V_0}{4\pi\lambda_c^3}\right)^{1/3} & \text{for } V_0 \leq \frac{4}{3}\pi\lambda_c^3 \text{ sphere,} \\ 2\lambda_c \left[1 - \frac{\pi}{4} + \sqrt{\left(\frac{\pi}{4}\right)^2 + \frac{2}{3}\left(\frac{3V_0}{4\pi\lambda_c^3} - 1\right)}\right] & \text{for } V_0 > \frac{4}{3}\pi\lambda_c^3 \text{ pancake,} \end{cases} \quad (3)$$

according to the initial volume  $V_0$  of a drop.

## C. EVAPORATION TIME AND COALESCENCE

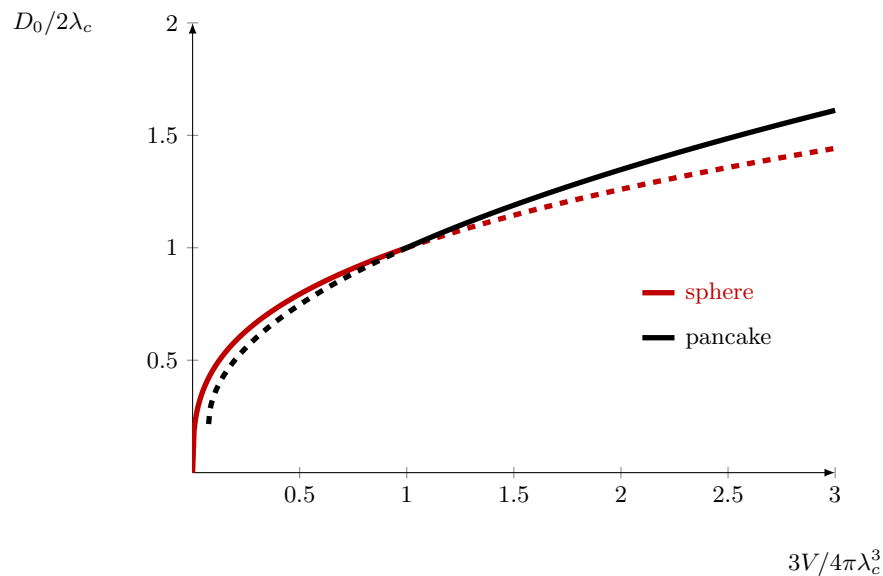


FIG. 1. Approximations of the initial diameter  $D_0$  of a drop as a function of the corresponding volume  $V$ . Normalization using the capillary length  $\lambda_c$  and the corresponding characteristic volume.

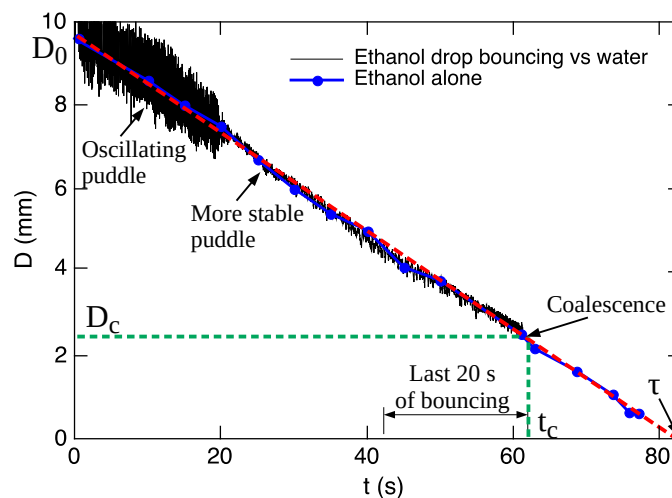


FIG. 2. Diameter  $D$  vs time  $t$  for a  $250 \mu\text{l}$  ethanol drop bouncing against a water drop during its evaporation on a plate at  $T_p = 250^\circ\text{C}$  (black line). In this case,  $t = 0$  corresponds to the initial deposition of the drop, with diameter  $D_0$ . The coalescence occurs at  $t = t_c \approx 63$  s. Blue points correspond to the evaporation process of an ethanol drop of the same initial volume deposited alone on the plate, with  $\tau \approx 83$  s of total evaporation time.

In Supplementary Fig. 2, the complete evaporation process for the case of an ethanol droplet bouncing against a Drop1 of water is shown, from the moment of drop deposition at  $t = 0$ , until its coalescence at  $t = t_c$ . The diameter of the ethanol drop  $D$  decreases linearly with time from its initial value  $D_0$  until the moment of coalescence, when  $D = D_c$ . The value of  $D(t)$  was obtained from the circular cross section measured from the top with a high speed camera at 125 fps. The noisy signal at the beginning of the process is due to the unstable shape of the ethanol drop when its volume is large. The droplet becomes more stable and adopts a puddle shape with circular cross section for values of  $D < 6$  mm. Note that the last 20 s of bouncing before coalescence shown in Fig. 4 (a-b) of our manuscript are only a fraction of the complete process. For comparison, we also present data of the evaporation of a single ethanol droplet (blue dots) of the same initial volume  $V_0 = 250 \mu\text{l}$ ,



deposited alone on the center on the center of the plate (without the presence of water drop). Note that the evaporation rate is practically the same, which is expected considering that the collisions between the droplets take only some milliseconds, and therefore, the effect on the evaporation rate is negligible. For the case of the single drop, we can obtain the values of  $D < D_c$ , and from the linear trend observed, one estimates the value of  $\tau \approx 83$  s.

Let us consider the observed linear decrease of  $D(t)$ , of the form:

$$D(t) = D_0 - kt , \quad (4)$$

where the slope  $k = D_0/\tau$  is a constant related to the evaporation rate. Then, the time of coalescence when  $D(t) = D_c$  can be written as:

$$t_c = \tau - D_c/k , \quad (5)$$

where  $\tau$  is the total evaporation time for a single drop of the same volume. Now, according to Sobac et al. [7], the lifetime of a single Leidenfrost drop is given by a power law relationship, described by:

$$\tau = aV_0^n , \quad (6)$$

where  $n$  and  $\log_{10}(a)$  are the slope and vertical intercept in a log-log scale, and  $\tau$  being the time measured since the beginning of the experiment. Combining the expression given in eq. (5), with the power law, described by eq. (6), yields:

$$t_c = aV_0^n - D_c/k , \quad (7)$$

As observed in Fig. 4c of the manuscript, the coalescence size  $D_c$  is largely independent of  $V_0$  for a given liquid, which leads to conclude that the coalescence time  $t_c$  has the same behavior as the lifetime  $\tau$ , but separated by a constant time lapse  $D_c/k$  from  $\tau$ .

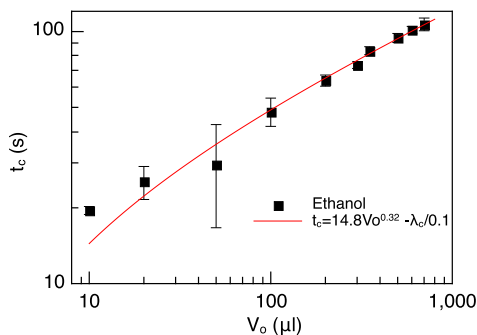


FIG. 3. Log-log plot of the coalescence time  $t_c$  of an ethanol drop with a water drop as a function of the initial volume of the ethanol drop  $V_0$ . The red line corresponds to the linear fit given by eq. (7).

Figure 3 shows the time of coalescence  $t_c$  as a function of the initial volume of the ethanol drop. The log-log plot reveals a power-law dependence, in agreement with Sobac et al. [7]. Since  $D_c$  was found to be of the order of the capillary length, one can use the value of  $\lambda_c$  for ethanol and the slope  $k$  obtained from the linear fit in Fig. 2 (red line) to fit the values of  $t_c$ . The fitting gives an exponent  $n = 0.32$ , which is close to  $1/3$ . This can be explained considering that  $D_0$  can be reasonably expressed as  $D_0 \propto V_0^{1/3}$  (see Fig. 1). Thus, one can write the fitting expression as:

$$t_c \approx AD_0 - \lambda_c/k , \quad (8)$$

in agreement with the linear dependence found in Fig. 2 and eq.(4) if one solves for  $t = t_c$  when  $D(t) = D_c$ .

## D. MODEL FOR THE TRIPLE LEIDENFROST EFFECT

For the configuration described in the manuscript, the force  $W_\phi$  that brings the droplets together is due to the projected weight of Drop2, which reads:

$$W_\phi \approx \rho_{l,2} V_2 g \phi , \quad (9)$$

where  $\rho_{l,2}$  and  $V_2$  are the density and volume of Drop2,  $g$  is the gravitational acceleration and  $\phi = \pi/90$  rad is the inclination angle of the plate. Between the droplets, a mixture layer of vapor from liquids that form both droplets will exist. This vapor comes from the regions L1 and L2, due to the Leidenfrost state of each drop, and should flow upwards through the gap between the drops, continuously and without stopping. Let's say that a uniform flow of vapor will flow between the drops.

Since the two droplets are made of different fluids, they present a different saturation temperature due to their Leidenfrost state. Considering that Drop2 presents a lower temperature than Drop1, *i.e.*  $T_2 < T_1$ , Drop1 may function as a hot surface for Drop2, which leads to a vapor generation per unit time from Drop2:

$$\dot{m}_{g2,L3} = \frac{A_{L3} k_{v,L3} \Delta T_{12}}{L_{lv2} e_{L3}} , \quad (10)$$

where  $\Delta T_{12} = T_1 - T_2$  is the temperature difference between drops,  $A_{L3}$  is the ‘‘contact’’ area of the region L3 between the drops,  $k_{v,L3}$  is the thermal conductivity of the vapor mixture layer,  $L_{lv2}$  is the latent heat of liquid 2, and  $e_{L3}$  being the distance between the drops, due to the mixture layer between them. The evaporation of Drop2 generates an additional amount of vapor that will also feed by mixture layer.

The projected weight force  $W_\phi$  exerts a pressure  $P_{L3} = W_\phi/A_{L3}$  over the L3 region of area  $A_{L3}$ . In turn, a radial flow of vapor is ejected from the ‘‘contact’’ zone and must be provoked by the pressure. Using the lubrication approximation, the ejection mass flow rate is given by:

$$\dot{m}_{out,L3} \approx \frac{2\pi \rho_{v,L3} (e_{L3})^3 W_\phi}{3 \eta_{v,L3} A_{L3}} , \quad (11)$$

where  $\rho_{v,L3}$  and  $\eta_{v,L3}$  are the density and dynamic viscosity of the vapor mixture layer, respectively.

Taking into account the vapor generation rate and the radial vapor flow, we can estimate the rate of change of the volume of the mixture layer as:

$$\frac{d}{dt} (\rho_{v,L3} A_{L3} e_{L3}) = \dot{m}_{g2,L3} - \dot{m}_{out,L3} . \quad (12)$$

For this balance, we do not consider the vapor that flows upwards from the L1 and L2 regions, since for a quasi-static analysis, the mass flow rate that enters the ‘‘contact’’ zone L3 should be similar to the mass flow rate that leaves this region. This is a simple view of the phenomenon, since we don't know exactly how the vapor coming from the L1 and L2 regions will enter and exit the L3 region.

Now, considering a linear elastic behavior of drops, in a series array, an effective radius of contact and a Hertzian-like behavior, the ‘‘contact’’ area is estimated by:

$$A_{L3} = \pi W_\phi R_{eff} \left( \frac{\sigma_1 + \sigma_2}{\sigma_1 \sigma_2} \right) \quad \text{with} \quad R_{eff} = 2 \left( \left[ \frac{\lambda_{c,1} + \lambda_{c,2}}{\lambda_{c,1} \lambda_{c,2}} \right] + \left[ \frac{R_1 + R_2}{R_1 R_2} \right] \right)^{-1} , \quad (13)$$

with the capillary lengths  $\lambda_{c,1} = \sqrt{\sigma_1/(g \rho_{l,1})}$  for Drop1 and  $\lambda_{c,2} = \sqrt{\sigma_2/(g \rho_{l,2})}$  for Drop2. This expression of the effective radius of contact comes from the assumption of the sizes of both drops, being larger than the corresponding capillary lengths. For a quasi-static situation, we can assume that the volumes of Drop1 and Drop2 will vary in a time scale that is much slower than that of the droplets relative motion. As a consequence, the vapor that is expelled from the regions L1 and L2 will flow with a slower speed than that of the vapor that is ejected from the L3 region, due to the approach of the droplets. Therefore, we can consider  $\rho_{v,L3}$ ,  $A_{L3}$ ,  $R_1$ ,  $R_2$  and  $V_2$  to be constant, which leads to:

$$\frac{de_{L3}}{dt} = \frac{C_1}{e_{L3}} - C_2 (e_{L3})^3, \quad (14)$$

with:

$$C_1 = \frac{k_{v,L3} \Delta T_{12}}{\rho_{v,L3} L_{lv2}} \quad \text{and} \quad C_2 = \frac{2}{3 \pi \phi \eta_{v,L3} g \rho_{l,2} V_2 (R_{eff})^2} \left( \frac{\sigma_1 \sigma_2}{\sigma_1 + \sigma_2} \right)^2. \quad (15)$$

If we define the initial thickness  $\varepsilon = e_{L3}(0)$  and a characteristic time  $\tau$ , together with the dimensionless variables  $e^* = e_{L3}/\varepsilon$  and  $t^* = t/\tau$ , the previously described ODE becomes:

$$\frac{de^*}{dt^*} = \frac{\tau C_1}{\varepsilon^2 e^*} - C_2 \tau \varepsilon^2 (e^*)^3. \quad (16)$$

Now, if we make  $\tau = 1/(C_2 \varepsilon^2)$  for dimensionless simplicity, then it becomes:

$$\frac{de^*}{dt^*} = \frac{C^*}{e^*} - (e^*)^3 \quad \text{with} \quad C^* = \frac{C_1}{C_2 \varepsilon^4}. \quad (17)$$

Considering the initial condition  $e^* = 1$  at  $t^* = 0$ , the solution of the ODE is given by:

$$e^* = \begin{cases} (C^*)^{1/4} \left\{ \tanh \left[ 2\sqrt{C^*} t^* + \tanh^{-1} \left( \frac{1}{\sqrt{C^*}} \right) \right] \right\}^{1/2} & \text{for } C^* > 0 \\ (2t^* + 1)^{-1/2} & \text{for } C^* = 0 \end{cases} \quad (18)$$

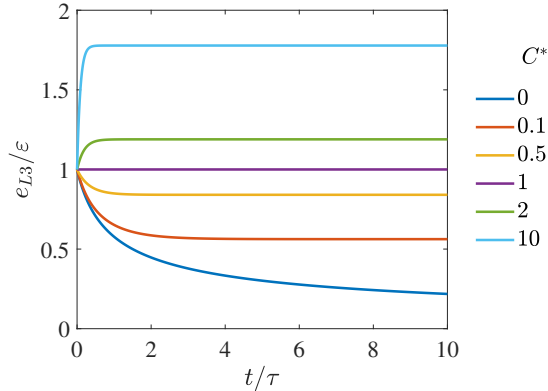


FIG. 4. Evolution of the thickness  $e_{L3}$  of the mixture layer in the L3 region (between Drop1 and Drop2) as a function of time  $t$ , for different values of the dimensionless parameter  $C^*$  (see eq. (17)). Normalization using the initial thickness  $\varepsilon$  and the corresponding characteristic time scale  $\tau = 1/(C_2 \varepsilon^2)$ .

In Fig. 4, we can observe that the thickness of the mixture layer will decrease if  $C^* < 1$ . For long times  $t^* \gg 1$ , we find that  $e^* \rightarrow C^*$ , thus:

$$e_{L3}(t \rightarrow \infty) = \frac{C_1}{C_2 \varepsilon^3}, \quad (19)$$

which also leads to the expression:

$$e_{L3}(t \rightarrow \infty) = \frac{3 \pi \phi}{2} \left( \frac{k_{v,L3} \eta_{v,L3}}{\rho_{v,L3}} \right) \left( \frac{g \rho_{l,2} \Delta T_{12}}{L_{lv2}} \right) \left( \frac{V_2 [R_{eff}]^2}{\varepsilon^3} \right) \left( \frac{\sigma_1 + \sigma_2}{\sigma_1 \sigma_2} \right)^2. \quad (20)$$

A priori, coalescence occurs when the mixture layer is drained and its thickness  $e_{L3}$  attains a critical value  $e_0 \sim 10$  nm, at which intermolecular forces become significant and the interfaces of the drops merge. Thus, the avoidance of coalescence should be observed when:

$$e_{L3}(t \rightarrow \infty) \geq e_0 \quad (21)$$

or equivalently:

$$V_2 (R_{eff})^2 \geq H \quad \text{with} \quad H = \frac{2 e_0 \varepsilon^3}{3 \pi \phi} \left( \frac{\sigma_1 \sigma_2}{\sigma_1 + \sigma_2} \right)^2 \left( \frac{L_{lv2}}{g \rho_{l,2} \Delta T_{12}} \right) \left( \frac{\rho_{v,L3}}{k_{v,L3} \eta_{v,L3}} \right). \quad (22)$$

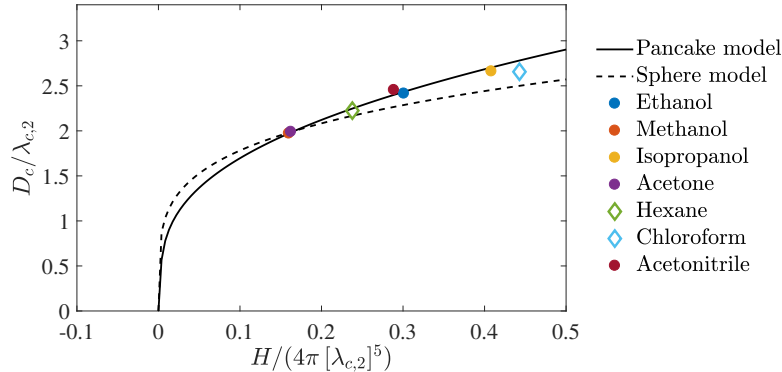


FIG. 5. Estimated coalescence diameter  $D_c$  of Drop2 as a function of the parameter  $H$ . Normalization using the capillary length  $\lambda_{c,2}$ . The continuous line corresponds to the solution of eq. (22) for the range  $H/(4\pi[\lambda_{c,2}]^5) \in [0, 0.8]$ , whereas the dots represent the solution of eq. (22) using the properties of different fluids (Drop2) and water (Drop1) to calculate the parameter  $H$ . For the model trend, a constant value of the capillary length  $\lambda_{c,2} = 1.6$  mm has been employed.

According to our model and the results presented in Fig. 5 (assuming a pancake-like shape for Drop2), the following conclusions can be drawn:

- If no temperature difference  $\Delta T_{12} = 0$  is present (corresponding to the  $C^* = 0$  case in the Fig. 4), the amount of vapor coming from the L1 and L2 regions is drained from region L3, and coalescence can not be avoided. Thus, to avoid coalescence  $\Delta T_{12} > 0$  should be established in order to make up for the ejected vapor.
- The effect of the plate temperature  $T_p$  is hidden in the last right-hand term of eq. (22). Additionally, as time goes on, the fraction of the vapor coming from the evaporation of Drop2 due to its approach with Drop1 (with flow rate  $\dot{m}_{g2,L3}$ ) will increase, and the properties of the vapor mixture will eventually become those of the vapor from Drop2, at a temperature  $(T_1 + T_2)/2$ .
- An estimate of the initial thickness of the vapor mixture layer should be provided. Our guess is that the drops will start their interaction at  $\varepsilon \approx 2(e_{L1} + e_{L2})$ , where  $e_{L1}$  and  $e_{L2}$  are the thicknesses of the vapor films at the regions L1 and L2, respectively. This thicknesses are calculated by using eq.(6) in Ref. [5]. The factor 2 has been taken from the observations of the expelled vapor from the bottom of Leidenfrost bodies, presented in Ref. [6].
- For the tested fluids, the coalescence diameter of Drop2 is in the range  $D_c/\lambda_{c,2} \in (2, 2.5)$ , which corresponds to the same order of magnitude of the experimental results presented in our manuscript.
- When Drop2 presents a higher temperature than Drop1, *i.e.*  $T_2 > T_1$ , Drop2 may function as a hot surface for Drop1, which leads to an inverse Leidenfrost effect. For this situation, one must use  $\Delta T_{21} = T_2 - T_1$  and  $L_{lv1}$  instead of  $\Delta T_{12}$  and  $L_{lv2}$ , respectively. Additionally, one must consider that the last right-hand term of eq. (22) should be determined with the properties of the vapor coming from the evaporation of Drop1, at a temperature  $(T_1 + T_2)/2$ .

- The results present in Fig. 5 were obtained considering that the drops may have a pancake-like shape, and its coalescence diameter should be  $D_c \geq 2\lambda_{c,2}$ . Since it might not always be the case, the expressions for the volume  $V_2$  and the effective radius  $R_{eff}$  can be modified for the spherical shape equivalents, if the coalescence diameter is expected to be  $D_c \leq 2\lambda_{c,2}$ . The corresponding trend is also presented in Fig. 5 as a dashed line.

- 
- [1] G. Vázquez, E. Alvarez, and J. M. Navaza, *Journal of Chemical & Engineering Data* **40**, 611 (1995).
  - [2] C. L. Yaws, *Chemical Properties Handbook* (McGraw-Hill Education, 1999).
  - [3] Engineering ToolBox, (2001). [online] <https://www.engineeringtoolbox.com>
  - [4] Merck KGaA. Merck solvent miscibility chart (2020); <https://www.sigmaaldrich.com/chemistry/solvents/solvent-miscibility-table.html> [last accessed 01 December 2020]
  - [5] A.-L. Bianco, C. Clanet, and D. Quéré, *Physics of Fluids* **15**, 1632 (2003).
  - [6] T. R. Cousins, R. E. Goldstein, J. W. Jaworski, and A. I. Pesci, *J. Fluid Mech.* **696**, 215–227 (2012).
  - [7] B. Sobac, A. Rednikov, S. Dorbolo, and P. Colinet, *Droplet Wetting and Evaporation* (Academic Press), pp. 85–99, 2015.
  - [8] L. Maquet, B. Sobac, B. Darbois-Textier, A. Duchesne, M. Brandenbourger, A. Rednikov, P. Colinet, and S. Dorbolo, *Phys. Rev. Fluids* **1**, 053902 (2016).